Computers and Concrete, *Vol. 11, No. 6 (2013) 493-513*
DOI: http://dx.doi.org/10.12989/cac.2013.11.6.493

The anchorage-slip effect on direct displacement-based design of R/C bridge piers for limiting material strains

P.E. Mergos*

Technological Educational Institute of Chalkida, Chalkida 34400, Greece

(Received October 25, 2011, Revised October 27, 2012, Accepted November 14, 2012)

Abstract. Direct displacement-based design (DDBD) represents an innovative philosophy for seismic design of structures. When structural considerations are more critical, DDBD design should be carried on the basis of limiting material strains since structural damage is always strain related. In this case, the outcome of DDBD is strongly influenced by the displacement demand of the structural element for the target limit strains. Experimental studies have shown that anchorage slip may contribute significantly to the total displacement capacity of R/C column elements. However, in the previous studies, anchorage slip effect is either ignored or lumped into flexural deformations by applying the equivalent strain penetration length. In the light of the above, an attempt is made in this paper to include explicitly anchorage slip effect in DDBD of R/C column elements. For this purpose, a new computer program named RCCOLA-DBD is developed for the DDBD of single R/C elements for limiting material strains. By applying this program, more than 300 parametric designs are conducted to investigate the influence of anchorage slip effect as well as of numerous other parameters on the seismic design of R/C members according to this methodology.

Keywords: seismic design; reinforced concrete; displacement-based; anchorage slip; material strains

1. Introduction

Current code provisions implement force-based procedures for seismic design of R/C structures. However, force-based design is against physical reality (Fardis 2009). It is known that damage is directly related to member deformations or lateral drifts (Priestley *et al.* 2007). Hence, displacement-based design represents a more rational approach for structural design against seismic demand.

A number of displacement-based methodologies have been developed for seismic design (fib Task Group 7.2 2003). One of the best-known procedures that falls within this category is the Direct Displacement Based Design (DDBD), which was initially developed by Priestley (1993) and Priestley and Kowalsky (2000). This approach, which connects directly the level of structural damage to the design strength, is well documented (Priestley 1993, Priestley *et al.* 2007), it is relatively easy to apply and well suited to incorporation in design codes (Calvi and Sullivan 2009).

The basic difference from force-based design is that DDBD models the structure by a SDOF system at peak displacement response rather than its elastic characteristics (Priestley Priestley *et al*.

*Corresponding author, Ph.D., E-mail: panmerg@yahoo.com

http://www.techno-press.org/?journal=cac&subpage=8 ISSN: 1598-8198(Print), 1598-818X (Online)

2007). This follows the Substitute Structure approach initially developed by Shibata and Sozen (1976). The fundamental concept of DDBD is to design a structure in order to achieve, rather than be bounded by, a given performance level for a given seismic action. The outcome of the procedure is the strength required at the plastic hinge regions to achieve the design goals in terms of pre-defined deformations or displacements (Priestley *et al*. 2007).

For DDBD, the performance limit state may be defined by either limiting material strains or lateral drifts. The former is the case when structural considerations are more critical since damage is strain-related for structural elements. The latter occurs when non-structural considerations control the design since damage to non-structural elements can be generally considered as drift-related (Priestley *et al*. 2007).

When designing an R/C column element according to DDBD for limiting concrete or steel strains, the design strength depends on the displacement demand of the member for these material strains. Since the displacement demand is influenced by the reinforcement content of its critical cross-section, an iterative procedure is generally required. Hence, the design process may become considerably time-consuming.

In this study, a new computer program, named RCCOLA-DBD, is developed, which automates, for the first time, the aforementioned design procedure for single R/C column members. By applying this design tool, the required design effort is minimized, while maximum accuracy is assured.

Furthermore, several experimental studies have shown that fixed end rotations caused by anchorage slip effect contribute significantly (up to 50%) to the total displacement capacity of an R/C member (Ma *et al.* 1976, Saatcioglu and Ozcebe 1989, Lehman and Moehle 1998). Since this displacement capacity represents the design displacement for DDBD for limiting deformations, it is evident that anchorage slip may play a vital role on the determination of the required design strength. Nevertheless, in all applications of DDBD until this moment, anchorage slip effect is either ignored or lumped into flexural deformations by applying the equivalent strain penetration length. As it will be shown later in this paper, this simplifying procedure may lead, in some cases, to erroneous results because it is not able to capture several aspects of the anchorage slip phenomenon. To resolve this controversy, it is proposed in this paper that anchorage slip effect is considered explicitly in the analytical procedure.

In the following, the procedure for determination of the force-displacement response of R/C members accounting explicitly for anchorage slip effect is described. Then, the methodology of DDBD for limiting material strains is outlined as well as its implementation in RCCOLA-DBD. Finally, more than 300 parametric designs are performed in order to investigate the influence of anchorage slip effect, as well as of numerous other design parameters, on the analytical results of DDBD of single R/C members for limiting material strains.

2. Force-displacement response of R/C members accounting explicitly for anchorage slip effect

One of the basic prerequisites of DDBD for limiting material strains is the derivation of the force-lateral displacement response of the R/C member under investigation. It is known that the total lateral tip displacement of an R/C cantilever can be considered as the sum of the displacements caused by flexural and shear deformations along its length as well as the displacement caused by the fixed-end rotation developed at its base due to anchorage slip effect.

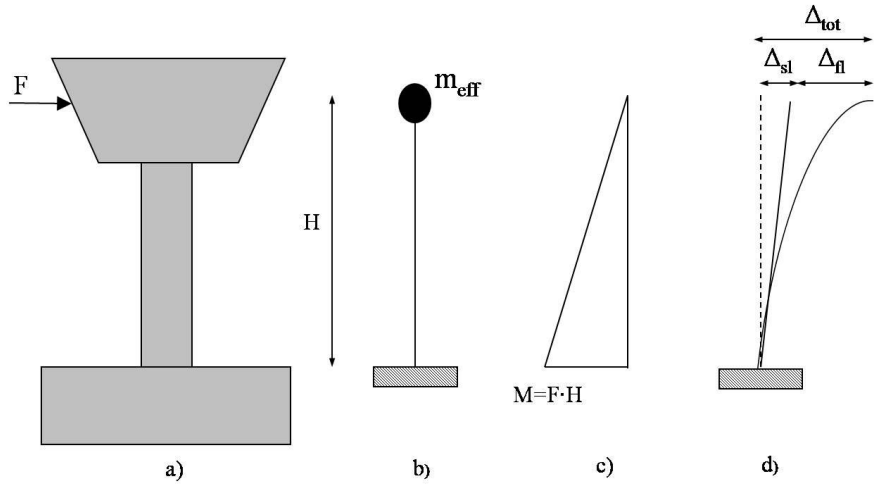

Fig. 1 Lateral deformation of an R/C cantilever: (a) R/C member, (b) SDOF representation, (c) moment diagram and (d) displacement profile

For relatively slender R/C members (aspect ratio greater than 3.0) with ductile detailing, shear deformations may be ignored with reasonable accuracy. It is noted that ignoring shear displacements is on the side of safety, when designing according to DDBD for limiting strains, since this reduces the displacement demand of the R/C member. For this reason, in the following, shear displacement is ignored. However, it is important to state that for the other R/C members shear deformations and shear-flexure interaction effect (Mergos and Kappos 2008, 2010, Beyer *et al.* 2011), should be taken into consideration in the design procedure.

Fig. 1 presents an R/C column cantilever as well as its SDOF representation. The most realistic structure conforming to the assumptions of a SDOF approximation is a regular bridge under transverse excitation. The height and effective mass of the cantilever are H and m_{eff} respectively. The cantilever is subjected to a lateral force F causing a bending moment $M=F\cdot H$ at its base.

The first step to define the displacement response of the R/C member is to perform a moment-curvature analysis of its critical cross-section. For this purpose, RCCOLA-DBD uses the well known program RCCOLA developed initially by Mahin and Bertero (1977) at UC Berkeley and later modified by Kappos (2002). For a given cross section, reinforcement, axial load N and strain at the extreme compression fibre ε_c the corresponding bending moment M and curvature φ are determined by applying an iterative procedure for the neutral axis depth c. This procedure is repeated for increasing levels of ε_c and the complete M-φ envelope curve of the cross-section under examination is determined for the given level of axial load.

Several constitutive material laws have been implemented in RCCOLA for the confined and unconfined concrete and the reinforcing steel under monotonic loading. In the following, the Kappos (1991) model for confined concrete and the Park and Sampson (1972) material law for reinforcing steel are assigned.

The strain limits for M-φ analysis depend on the design limit state. For the damage control limit state the limit to confined concrete compression strain ε_{cu} is usually taken to occur when fracture of the transverse reinforcement confining the core takes place. For this state, the Mander *et al.* (1986) criterion is adopted herein given by Eq. (1), where ρ_w, f_{yw} and $\varepsilon_{sw,ult}$ are the volumetric ratio,

yield strength and strain at maximum strength of the transverse reinforcement and f_{cc} is the maximum strength of the confined concrete. The limit to the extreme tension reinforcement strain may be taken as a predefined value (e.g. 0.05) or as a fraction of the strain at maximum stress ε_{su} (e.g. $0.6\varepsilon_{su}$). Apparently, the ultimate curvature φ_u and moment M_u capacity are determined by the minimum values corresponding to one of these strain limits.

$$\varepsilon_{cu} = 0.004 + 1.4 \cdot \frac{\rho_w \cdot f_{yw} \cdot \varepsilon_{sw,ult}}{f_{cc}} \tag{1}$$

For design purposes, it is generally sufficient to adopt a bilinear approximation of the actual M-φ response (Fig. 2(a)). In this study, the respective methodology described analytically in Priestley *et al.* (2007) is adopted. Following this analytical procedure, the equivalent yielding moment M_y and curvature φ_y are determined.

It is known that the calculation of the top displacement response of an R/C cantilever by integrating the curvature profile derived by the moment diagram and the M-φ analysis described in the preceding paragraphs does not agree with the experimental observations. This is due to the tension shift, anchorage slip and shear deformation effects.

To overcome these difficulties, typically, the concept of the equivalent plastic hinge length L_p is adopted (Paulay and Priestley 1992), over which the curvature is assumed to be constant and equal to the respective value at the cantilever base. The curvature distribution outside this length is assumed to be linear. This compensates for tension shift effect and partially for shear deformations (Priestley *et al.* 2007).

The plastic hinge length incorporates the strain penetration length L_{sp}, which aims at accounting for the fixed end rotation caused by anchorage slip effect. Hence, L_p is given by Eq. (2), where k factor accounts for strain hardening effect.

$$L_p = k \cdot H + L_{sp} \geq 2 \cdot L_{sp} \tag{2}$$

Various relationships (fib Chapter 4) can be found in the literature for k and L_{sp}. Herein, the proposals by Priestley *et al.* (2007) are adopted, as shown in the following equations, where f_{yl}, f_{ul} and d_{bl} are the yield and ultimate strength and bar diameter of the longitudinal reinforcement.

$$L_{sp} = 0.022 \cdot f_{yl} \cdot d_{bl} \tag{3}$$

$$k = 0.2 \cdot \left(\frac{f_{ul}}{f_{yl}} - 1 \right) \leq 0.08 \tag{4}$$

Following the concept of the plastic hinge length, the cantilever tip displacements at yielding Δ_y and ultimate Δ_u states are given by Eqs. (5) and (6) respectively.

$$\Delta_y = \varphi_y \cdot \left(H + L_{sp} \right)^2 / 3 \tag{5}$$

$$\Delta_u = \Delta_y + \left(\varphi_u - \varphi_y \right) \cdot L_p \tag{6}$$

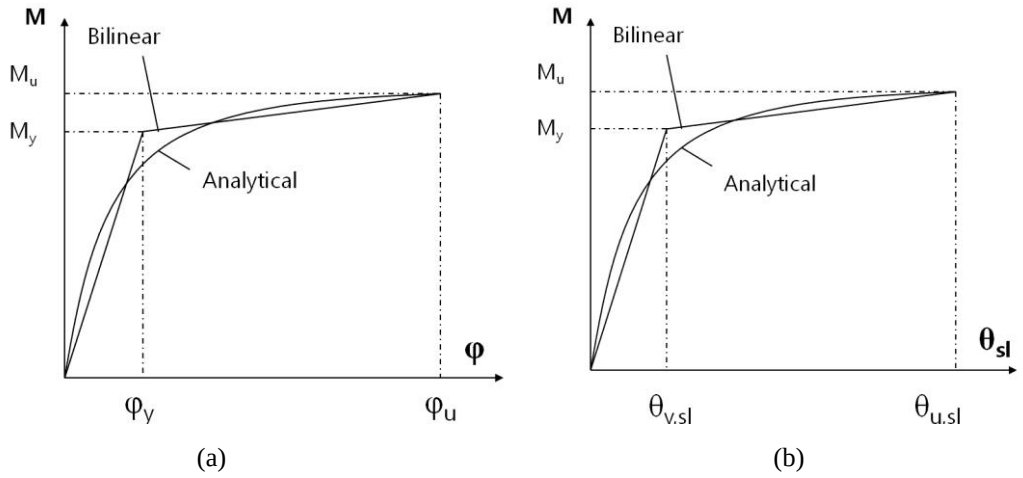

Fig. 2 Bilinear approximations: (a) moment-curvature and (b) moment-anchorage slip rotation envelopes

It can be inferred from the above that the fixed end rotations caused by anchorage slip effect are taken indirectly into account in the calculations by the empirical strain penetration length L_{sp} and the results of M-φ analysis of the critical cross section. However, as it will be shown later on, in this way various parameters affecting anchorage slip like bond strength, hardening of the reinforcing steel, anchorage detailing cannot be captured with sufficient accuracy. This issue becomes more important for DDBD for limiting material strains, since fixed end rotations may influence significantly the displacement demand of the R/C member for these material strains and consequently the design strength of its critical cross section.

For this reason, it is proposed herein that anchorage slip is included explicitly in the design procedure. Various analytical methodologies have been developed so far for the determination of fixed-end rotations caused by anchorage slip effect (Otani and Sozen 1972, Filippou 1985, Alsiwat and Saatcioglu 1992, Lowes and Altoontash 2003, Sezen and Setzler 2008). Herein, the Alsiwat and Saatcioglu (1992) analytical procedure is adopted, which has been proven to provide adequate correlation with the experimental evidence, while it remains simple enough in order to be easily incorporated in seismic design of R/C members.

According to this methodology, the moment-anchorage slip rotation (M-θ_{sl}) skeleton curve is derived on the basis of assuming uniform bond stress distribution along different segments of the anchored rebar (Fig. 3(d)). These segments are the elastic region L_e, the strain-hardening region L_{sh} and the pullout cone region L_{pc}. Following the experimental observations of Lehman and Moehle (1998) regarding well confined concrete bridge columns, the average bond strength τ_{be} is taken here equal to $1.0\sqrt{f_c}$ for the elastic region and the bond resistance τ_{bf} corresponding to L_{sh} equal to $0.5\sqrt{f_c}$. The same values have been assigned by Sezen and Setzler (2008) providing adequate match with the experimental recordings. In the pullout cone region, it is assumed that the acting bond is negligible.

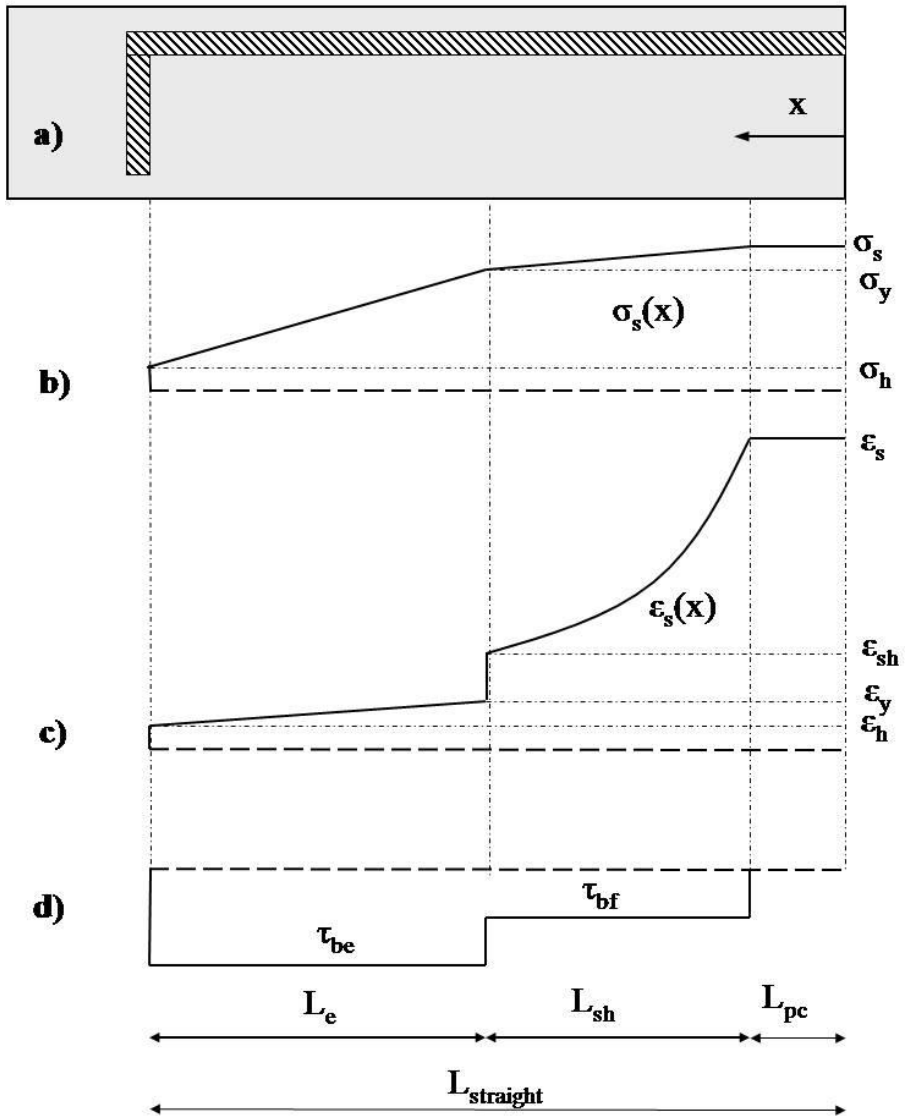

Fig. 3 (a) Reinforcing bar with 90° hook embedded in concrete, (b) steel stress distribution, (c) strain distribution and (d) bond stress distribution

For various levels of the applied end moment and using the results of *M-φ* analysis, the stress σ_s and strain ε_s of the reinforcing bar at the loaded end are first determined. Then, from equilibrium and applying the assumed bond distribution, variation of reinforcing bar stress $\sigma_s(x)$ along the embedment length is defined as shown in Fig. 3(b), where σ_y is the yield strength of steel and σ_h is the stress at the end of the straight part of the rebar anchorage. Then, by assigning an appropriate constitutive material law for steel (Park and Sampson 1972), strain distribution $\varepsilon_s(x)$ is determined, as shown in Fig. 3(c), where ε_y and ε_{sh} are the steel strains at the onset of yielding and strain

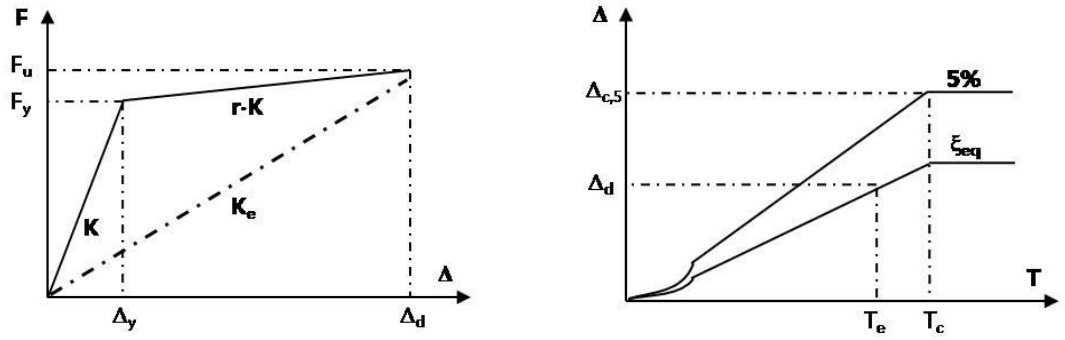

(a) (b)

Fig. 4 (a) Effective stiffness K_e of the equivalent SDOF system at peak response and (b) design displacement spectra

hardening, respectively, and ε_h is the steel strain at the end of the straight part of the anchorage. It is important to note that post-yield nonlinearity of the material constitutive law, i.e., strain hardening, should be taken into account because it affects significantly the final results (Mergos 2011).

Once $\varepsilon_s(x)$ is determined, slip of the reinforcement δ_{slip} can be calculated by integration along the anchorage length of the bar. In the case of hooked bars, local slip of the hook should be added. This can be evaluated by the force acting on the hook $P_h=A_b\cdot\sigma_h$, where A_b is the area of the anchored bar, and an appropriate hook force vs. hook slip relationship (Soroushian *et al.* 1988).

Upon determination of δ_{slip}, the respective fixed-end rotation can be calculated by Eq. (7), where $(d\text{-}x_c)$ is the distance between the bar and the neutral axis. The envelope $M\text{-}\theta_{sl}$ curve constructed by the various points of the afore-described methodology is then idealized by a bilinear relationship for the purposes of analysis (Fig. 2(b)). It is noted that since the reinforcement anchorage is designed to avoid brittle pullout failure, it can be assumed that the failure point ($\theta_{u,sl}$, M_u) of the bilinear $M\text{-}\theta_{sl}$ curve corresponds to the ultimate point of the bilinear $M\text{-}\varphi$ curve (φ_u, M_u). For reasons of simplicity, it is assumed herein that the bilinearization technique of the $M\text{-}\theta_{sl}$ envelope follows the respective method of the $M\text{-}\varphi$ envelope curve. This effectively means that both bilinear envelopes yield at the same equivalent yielding moment M_y (Fig. 2).

$$\theta_{sl} = \frac{\delta_{slip}}{d - x_c} \tag{7}$$

By modelling explicitly fixed end rotations caused by anchorage slip, the cantilever tip displacements at yielding Δ_y and ultimate Δ_u states are now given by Eqs. (8) and (9) respectively.

$$\Delta_y = \varphi_y \cdot H^2/3 + \theta_{y,sl} \cdot H \tag{8}$$

$$\Delta_u = \Delta_y + \left(\varphi_u - \varphi_y\right) \cdot k \cdot \left(1 - k/2\right) \cdot H^2 + (\theta_{u,sl} - \theta_{y,sl}) \cdot H \tag{9}$$

3. Direct displacement-based design for limiting material strains formulation

The vertical R/C cantilever structure of Fig. 1(a) is represented by the SDOF system of Fig. 1(b). The bilinear envelope of the lateral force-displacement response of the SDOF representation is shown in Fig. 4(a), where an initial stiffness K is followed by a post yield stiffness $r \cdot K$.

DDBD characterizes the structure by secant stiffness K_e at maximum displacement Δ_d and a level of equivalent viscous damping ξ_{eq} representative of the combined elastic damping and the hysteretic energy absorbed during inelastic response (Priestley *et al*. 2007).

The first step of DDBD for limiting concrete and steel strains ε_{cd} and ε_{sd} is the computation of the yield Δ_y and design displacement Δ_d for these strain limits. This can be achieved by Eqs. (5), (6), (8), and (9) by setting φ_u and $\theta_{u,sl}$ equal to the design curvature φ_d and fixed-end rotation $\theta_{d,sl}$ corresponding to the most critical strain among ε_{cd} and ε_{sd}.

Nevertheless, it is evident from these equations that for calculation of Δ_y and Δ_d the reinforcement configuration should be predefined. Hence, in general, an iterative procedure is required, which may increase considerably the computational effort. In this study, this procedure is automated by developing the computer program RCCOLA-DBD as described in the following.

The equivalent viscous damping ξ_{eq} is determined as a function of the displacement ductility demand $\mu_d = \Delta_d/\Delta_y$. Different equations have been proposed (Grant *et al.* 2005, Dwairi *et al*. 2007) for estimating ξ_{eq} by μ_d depending on the structural type. Herein, the following equation is applied, as proposed by Dwairi *et al.* (2007) for concrete wall buildings and bridges.

$$\xi_{eq} = 0.05 + 0.444 \cdot \left(\frac{\mu_d - 1}{\pi \cdot \mu_d} \right) \tag{10}$$

With the design displacement Δ_d determined and the corresponding ξ_{eq} damping estimated from μ_d, the effective period T_e at maximum response can be read from a set of displacement spectra for different levels of damping, as shown in Fig. 4(b). In this figure, a typical design displacement spectra set for damping levels 5% and ξ_{eq} is presented. Displacements for the 5% spectrum increase with period up to a value $\Delta_{c,5}$ corresponding to the corner period T_c. For normal accelerograms measured at least 10 km from the fault rupture, the displacements $\Delta_{T,\xi}$ corresponding to a different level of damping ξ_{eq} can be related to the displacements for 5% damping $\Delta_{T,5}$ by the EC8 expression

$$\Delta_{T,\xi} = \Delta_{T,5} \cdot \left(\frac{0.10}{0.05 + \xi_{eq}} \right)^{0.5} \tag{11}$$

In the following, the small nonlinearity at low periods of the displacement spectra is ignored since it is unlikely to be significant for displacement-based designs, where the effective period at maximum response is typically very high (Priestley *et al*. 2007). By this assumption, for the design displacement Δ_d and equivalent damping ξ_{eq}, the effective period T_e is calculated by the respective displacement spectrum (Fig. 4(b)) as

$$T_e = T_c \cdot \frac{\Delta_d}{\Delta_{c,5}} \cdot \left(\frac{0.05 + \xi_{eq}}{0.10} \right)^{0.5} \tag{12}$$

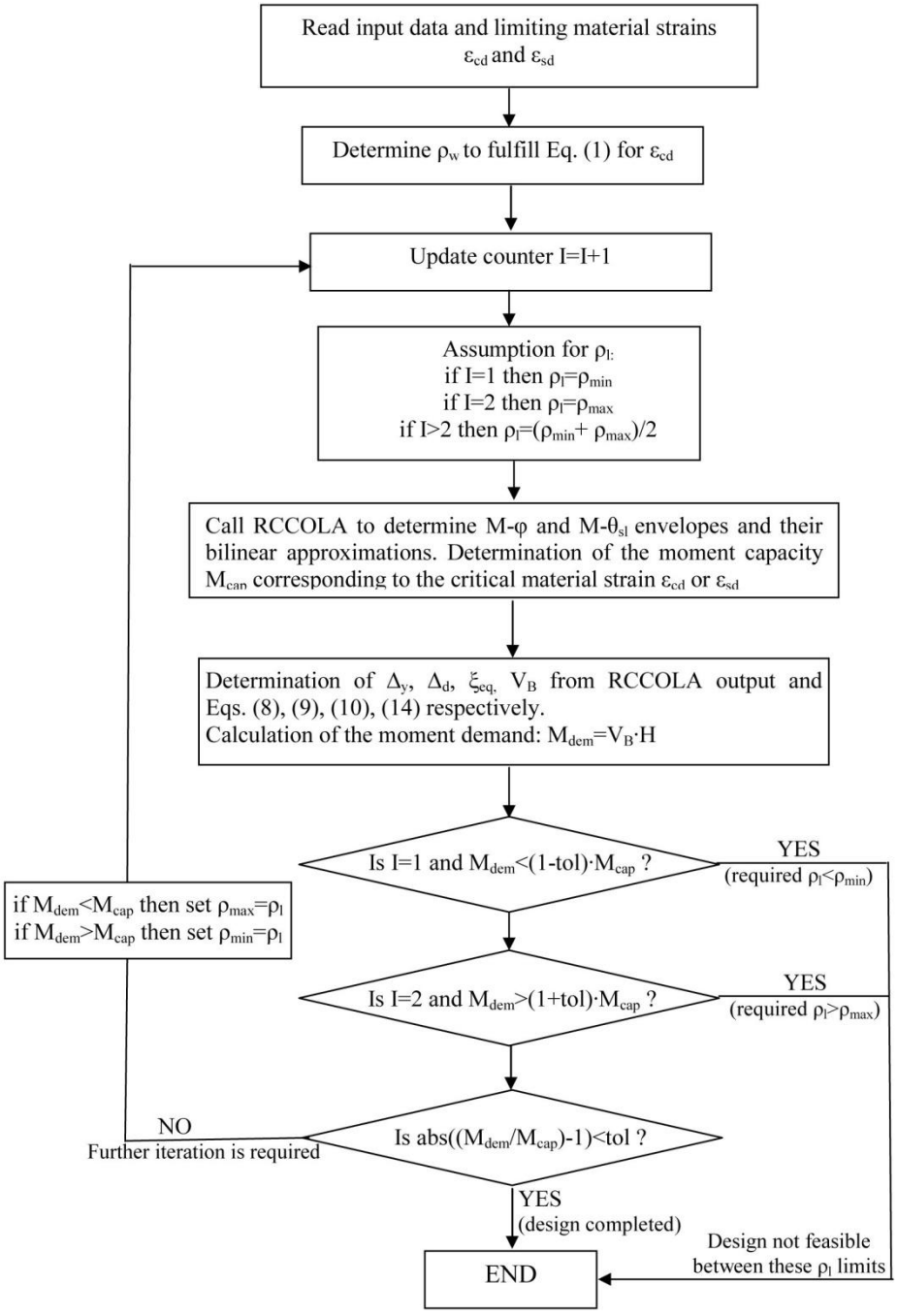

Fig. 5 RCCOLA-DBD flowchart

The effective stiffness K_e at peak response is given by

$$K_e = \frac{4 \cdot \pi^2 \cdot m_e}{T_e^2} = \frac{4 \cdot \pi^2 \cdot m_e}{T_c^2} \cdot \frac{\Delta_{c,5}^2}{\Delta_d^2} \cdot \left(\frac{0.10}{0.05 + \xi_{eq}} \right) \tag{13}$$

Finally, the design base shear V_B is determined as

$$V_B = K_e \cdot \Delta_d = \frac{4 \cdot \pi^2 \cdot m_e}{T_c^2} \cdot \frac{\Delta_{c,5}^2}{\Delta_d} \cdot \left(\frac{0.10}{0.05 + \xi_{eq}} \right) \tag{14}$$

Upon determination of V_B, the design moment of the critical cross-section $M_{dem}=V_B \cdot H$ is defined. Then, the longitudinal reinforcement of this section is determined in order to yield this moment capacity for the given level of axial load and the critical limiting material strain ε_{cd} or ε_{sd}.

The transverse reinforcement may be given a predefined configuration for construction reasons but in any case it should be adequate to assure the design concrete limiting material strain ε_{cd} as determined by Eq. (1). For this calculation, a short iterative procedure is required since the confined concrete strength f_{cc} is also a function of the transverse reinforcement volumetric ratio ρ_w.

In some cases, the procedure described above may require considerable computational effort since the displacement demand Δ_d and consequently the design shear V_B of the R/C member depends on its reinforcement content. Nevertheless, effective design tools have not yet been developed to simplify this methodology.

In this study, this design methodology is automated by developing the computer software RCCOLA-DBD. RCCOLA-DBD utilizes the well-known program RCCOLA (Mahin and Bertero 1977) for the M-φ analysis of the critical cross-section of the R/C cantilever under examination. An additional subroutine has been introduced in RCCOLA by the writer of this paper (Mergos 2011) to perform the M-θ_{sl} analysis, following the procedure (Alsiwat and Saatcioglu 1992) described in the preceding section. Furthermore, additional lines have been written for the bilinearization of the analytical M-φ and M-θ_{sl} envelopes according to the Priestley *et al.* (2007) methodology.

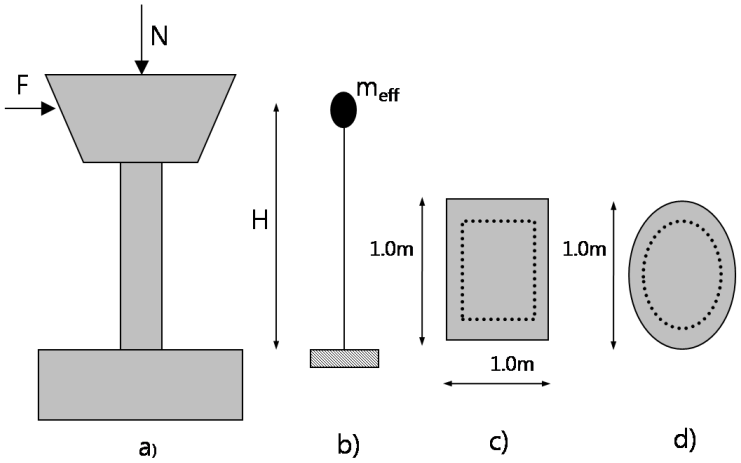

Fig. 6 Basic design case study: (a) R/C bridge pier, (b) SDOF representation, (c) square cross-section and (d) circular cross-section

The flowchart of RCCOLA-DBD is presented in Fig. 5. Required data are the R/C cantilever geometry, material properties, limiting material strains, design displacement spectra, reinforcing bars distribution, anchorage detailing, maximum ρ_{max} and minimum ρ_{min} allowable volumetric ratios of the critical section longitudinal reinforcement and the allowable design moment tolerance tol. The outcomes of RCCOLA-DBD are the required longitudinal ρ_l and transversal ρ_w reinforcement volumetric ratios. As it can be seen in Fig. 5, RCCOLA-DBD employs the interval bisection root solution algorithm for the determination of ρ_l. Depending on the comparisons between moment demand M_{dem} and moment capacity M_{cap}, the program narrows the ρ_l solution limits until convergence between M_{dem} and M_{cap} is achieved with the pre-specified tolerance *tol*. Following this analytical procedure, RCCOLA-DBD minimizes the required design effort, while it assures maximum computational accuracy.

4. Design applications

4.1 Basic design example

In this section, the basic design example is described. This case study is used as reference, in the next section, for numerous parametric designs aiming at illustrating the influence of various parameters on the outcome of DDBD for limiting material strains.

The basic case study is shown in Fig. 6. It is an R/C bridge pier with a 1.0 m square or circular cross-section. The longitudinal reinforcement is assumed evenly distributed around the perimeter. The cover to flexural reinforcement is taken 50 mm. The height of the cantilever is H=5.0 m. The yield strength f_{yl}, strain hardening f_{ul}/f_{yl}, strain at maximum strength ε_{su} and bar diameter d_{bl} of the longitudinal reinforcement are 500 MPa, 1.35, 0.15 and 20 mm respectively. The yield strength and strain at maximum strength $\varepsilon_{sw,ult}$ of the transverse reinforcement are also assumed 500 MPa and 0.15. Concrete strength f_c is 30 MPa and the anchorage is assumed to be straight (without end-hook).

For both sections to yield similar results, it is assumed that the axial load ratios of the square and the circular cross-sections are 0.13 and 0.10 respectively. The corner period T_c and displacement $\Delta_{c,5}$ of the 5% displacement spectrum are taken as 4.0 sec and 0.6 m. Finally, the limiting material strains for concrete ε_{cd} and steel ε_{sd} are taken equal to 0.015 and 0.05 respectively.

Table 1 summarizes the iterative design procedure performed by RCCOLA-DBD for the basic design example and the circular cross-section. The M_{dem}/M_{cap} ratio tolerance is specified equal to 1%. The ρ_l limits ρ_{min} and ρ_{max} are set initially equal to 0.2% and 8%. Of course, these limits are not allowed for construction reasons, but they are chosen herein to cover all possible parametric designs of the following section. Convergence is achieved after 8 iterations. It is worth noting that the 4th iteration is very close to convergence (error approximately 3%), but in order to fulfill the strict pre-specified tolerance (1%) further iterations are necessary. If narrower ρ_l limits we chosen, the convergence would be faster. The final required longitudinal reinforcement volumetric ratio is calculated as 2.03%. The necessary transverse reinforcement ratio to achieve ε_{cd}=0.015 is ρ_w=0.34%.

Similar calculations for the square cross-section yield that the required longitudinal reinforcement is ρ_l=2.27%.

Table 1 Iterative design procedure for the basic design example and the circular cross-section

Iteration/parameter	1	2	3	4	5	6	7	8
ρ_{min} (%)	0.2	0.2	0.2	0.2	0.2	1.175	1.663	1.906
ρ_{max} (%)	8.0	8.0	8.0	4.1	2.15	2.15	2.15	2.15
ρ_l (%)	0.2	8.0	4.1	2.15	1.175	1.663	1.906	2.028
φ_y (rad/m)	0.0046	0.0061	0.0060	0.0057	0.0054	0.0055	0.0056	0.0056
$\theta_{y,sl}$ (rad)	0.00098	0.00114	0.00125	0.00119	0.00113	0.00116	0.00118	0.00118
φ_d (rad/m)	0.0675	0.0361	0.0407	0.0467	0.0534	0.0494	0.0479	0.0473
$\theta_{sl,d}$ (rad)	0.0110	0.00409	0.00496	0.00626	0.00774	0.00684	0.00652	0.00638
Δ_y (m)	0.043	0.057	0.056	0.053	0.050	0.052	0.053	0.053
Δ_d (m)	0.200	0.122	0.133	0.148	0.164	0.154	0.151	0.149
μ_Δ	4.608	2.148	2.376	2.776	3.271	2.970	2.864	2.819
ξ_{eq}	0.161	0.126	0.132	0.140	0.148	0.144	0.142	0.141
T_e (sec)	1.935	1.079	1.198	1.361	1.542	1.433	1.393	1.376
V_B (kN)	496.01	974.61	862.40	741.77	641.60	698.52	721.70	732.28
M_{dem} (kNm)	2480.07	4873.08	4312.01	3708.85	3208.02	3492.61	3608.50	3661.42
M_{cap} (kNm)	1255.59	10592.4	6144.71	3828.90	2600.65	3223.87	3527.63	3680.32
M_{dem}/M_{cap}	1.975	0.460	0.702	0.969	1.234	1.083	1.023	0.995

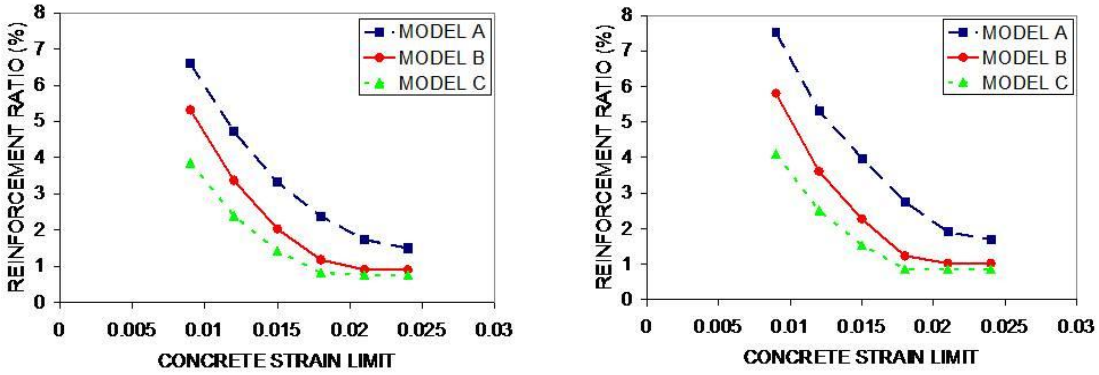

(a) (b)

Fig. 7 Variation of the longitudinal reinforcement demand with the limiting concrete strain ε_{cd} for the (a) circular and (b) square cross-section

4.2 Parametric designs

In this section, parametric designs are conducted according to the DDBD for limiting material strains methodology and by the application of RCCOLA-DBD. The design example of the previous section serves as the basis for this parametric study. In each case, one design parameter of this example is modified in order to investigate its effect on the final outcome of DDBD.

In addition, to examine the influence of anchorage slip effect, three different models are applied in the analytical procedure. The A model considers only flexural deformations in the calculation of Δ_y and Δ_d. Hence, anchorage slip effect is totally disregarded for this model. The B model (proposed model) takes explicitly anchorage slip effect through the procedure described previously

in this study. Finally, C model accounts for anchorage slip effect by the application of Eq. (2) for the plastic hinge length, as proposed by Priestley *et al.* (2007).

It is important to note that in all cases, T_{eff} remains always lesser than T_c (hence Eq. (14) always holds) and the lateral drift limit does not exceed 0.045. The analytical results of the parametric study are presented in the following.

4.2.1 The limiting concrete strain ε_{cd}

Herein, the variation of longitudinal reinforcement demand is examined with the limiting concrete strain ε_{cd}. For this reason, the basic design example is solved for six different values of ε_{cd}=0.009, 0.012, 0.015, 0.018, 0.021 and 0.024. The required ρ_w to achieve these strains are 0.15%, 0.24%, 0.34%, 0.44%, 0.54% and 0.65% respectively. However, ρ_w was not taken lesser than 0.22% and 0.30% for the circular and the rectangular cross-section respectively corresponding to single stirrups ø8/10.

It is evident from Fig. 7 that ρ_l demand increases significantly as the limiting ε_{cd} decreases. This is rational since smaller ε_{cd} means less damage for the R/C member. It is worth noting that models

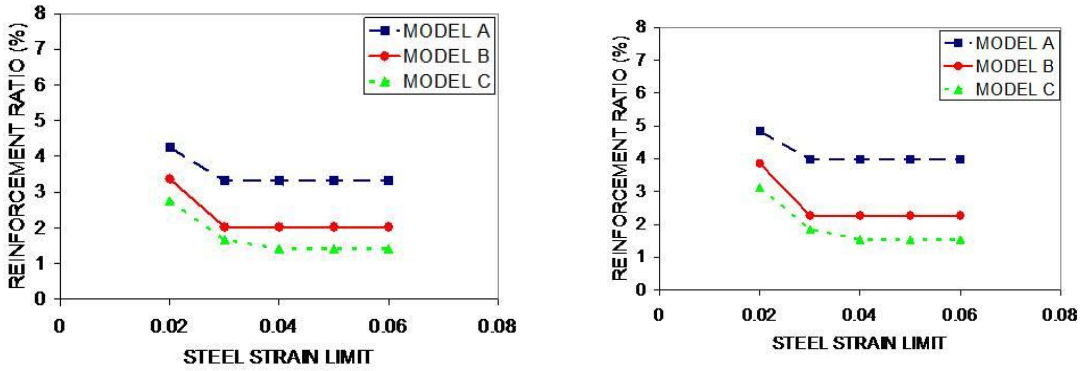

(a) (b)

Fig. 8 Variation of the longitudinal reinforcement demand with the limiting steel strain ε_{sd} for the (a) circular and (b) square cross-section

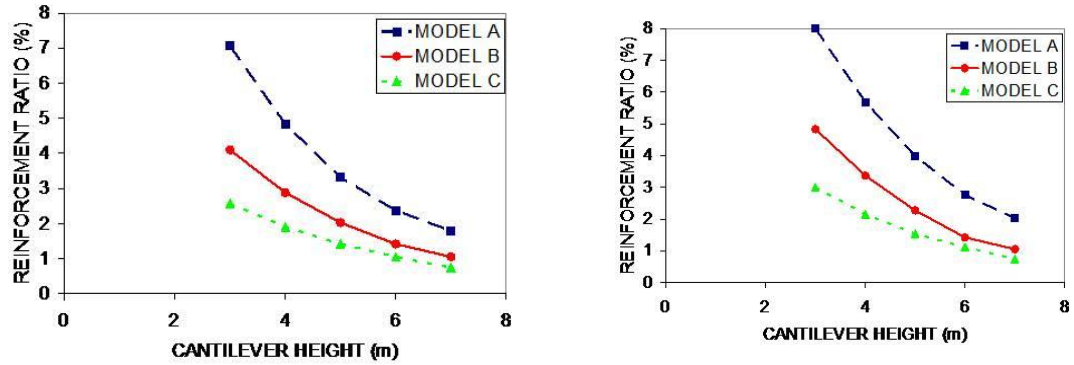

(a) (b)

Fig. 9 Variation of the longitudinal reinforcement demand with the cantilever height H for the (a) circular and (b) square cross-section

B and C predict the same ρ_l demand for ε_{cd}=0.021 and 0.024. This is because, for these models and concrete strains, the steel limiting strain ε_{sd}=0.05 becomes more critical than ε_{cd}.

Furthermore, from the comparisons of the results of models A, B and C, it is concluded that anchorage slip effect plays a vital role on the determination of ρ_l. In some cases, model A, which ignores anchorage slip effect, yields up to 3 times more longitudinal reinforcement demand than model C. Models B and C tend to coincide as ε_{cd} increases, but they provide considerably different predictions for small values of ε_{cd}. For these design examples, model B yields safer designs than model C.

4.2.2 The limiting steel strain ε_{sd}

Herein Fig. 8, the variation of longitudinal reinforcement demand is examined with the limiting

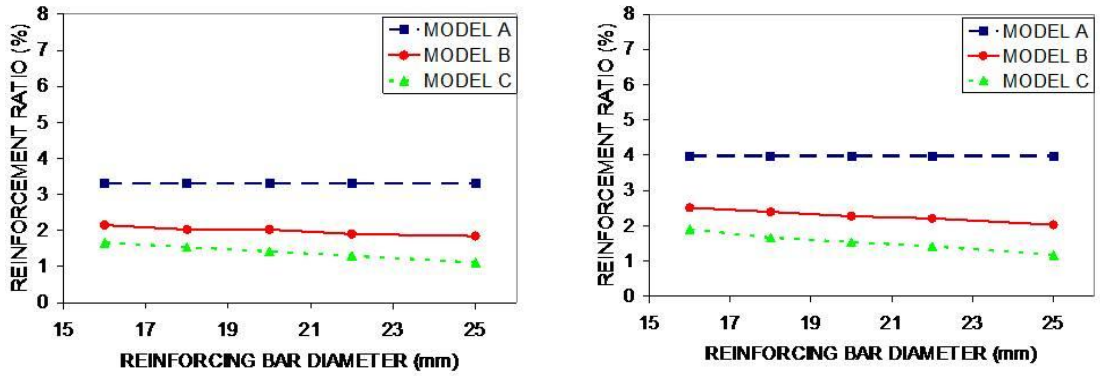

Fig. 10 Variation of the longitudinal reinforcement demand with the reinforcing bar diameter d_{bl} for the (a) circular and (b) square cross-section

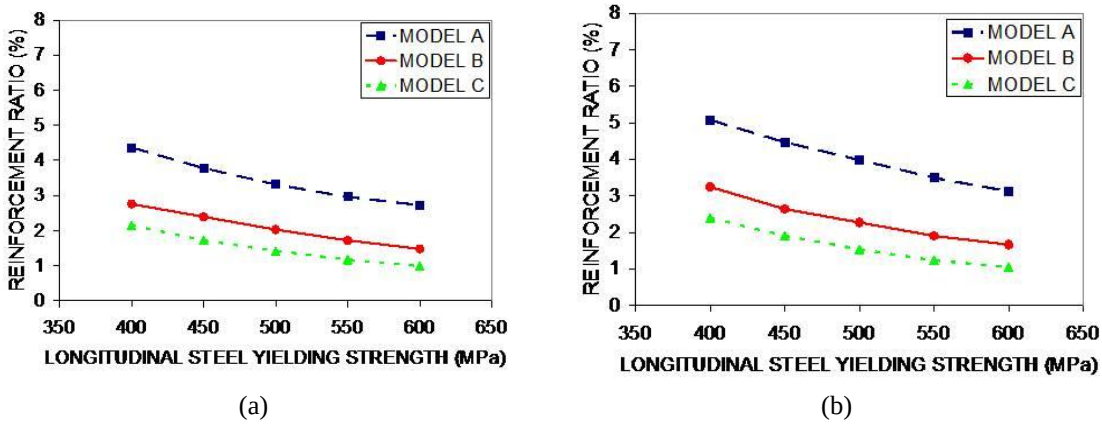

Fig. 11 Variation of the longitudinal reinforcement demand with the reinforcing bar yielding strength f_{yl} for the (a) circular and (b) square cross-section

steel strain ε_{sd}. For this reason, the basic design example is solved for five different values of ε_{sd}=0.02, 0.03, 0.04, 0.05 and 0.06. It can be seen that ρ_l demand decreases as ε_{sd} increases. This is expected since more damage is accepted in this manner. However, when ε_{sd} becomes higher than 0.03 for models A and B and 0.04 for model C, ρ_l demand remains constant since concrete limiting strain ε_{cd}=0.015 is more critical in these cases.

4.2.3 The cantilever height H

To investigate the influence of the cantilever height H on ρ_l demand, the basic design example is solved for five different heights H=3 m, 4 m, 5 m, 6 m and 7 m. 'In Fig. 9 It is clear that as H increases, ρ_l demand decreases. This is due to the fact that the displacement demand of the R/C member for the same limiting material strains increases as its height increases. It is important to note that as H increases the deviation of the three different models A, B and C decreases. This happens because as H increases flexural deformations govern the response and anchorage slip effect becomes less important.

4.2.4 The reinforcing bars diameter d_{bl}

The reinforcing bars diameter d_{bl} is a parameter influencing solely anchorage slip of the R/C member. As d_{bl} increases anchorage slip becomes more important. To investigate the influence of d_{bl} on ρ_l demand, the basic design example is solved for five different bar diameters d_{bl}=16 mm, 18 mm, 20 mm, 22 mm and 25 mm. It can be seen in Fig. 10 that while model A predicts the same ρ_l for all bar diameters, models B and C clearly show that ρ_l demand decreases as d_{bl} increases since anchorage slip effect becomes more important. Model B predicts approximately 20% decrease in ρ_l demand as d_{bl} increases from 16 mm to 25 mm. In the same case, model C predicts approximately 40% decrease in ρ_l demand.

4.2.5 The reinforcing bars yielding strength f_{yl}

To examine the influence of the reinforcing bars yielding strength f_{yl} the basic design example is solved for five different values of f_{yl}=400 MPa, 450 MPa, 500 MPa, 550 MPa and 600 MPa. As shown in Fig. 11, ρ_l demand decreases significantly as the yielding strength increases. This is the case for all models A, B and C employed herein.

4.2.6 The reinforcing bars strain hardening f_{ul}/f_{yl}

Apart from the steel yielding strength f_{yl}, the steel strain hardening f_{ul}/f_{yl} strongly affects fixed end rotations caused by anchorage slip. This is due to the fact that strain hardening determines the strain-hardening anchorage length L_{sh} (Fig. 3), where inelastic deformations concentrate. Typically, this region creates the major part of the fixed end rotations caused by anchorage slip.

To examine the influence of $f_{ul}/f_{yl,}$ the basic design example is solved for five values of f_{ul}/f_{yl}=1.15, 1.25, 1.35, 1.45 and 1.55. The yielding strength f_{yl} remains 500 MPa. In Fig. 12, it can be seen that ρ_l demand, as predicted by models A and C, remains almost constant with the variation of strain hardening. However, model B is the only model able to capture that as strain hardening increases L_{sh} and consequently fixed end rotation also increase causing higher values of Δ_d and consequently lower ρ_l demands. This emphasizes the need for explicitly modeling anchorage slip effect, when designing according to the DDBD methodology for limiting material strains.

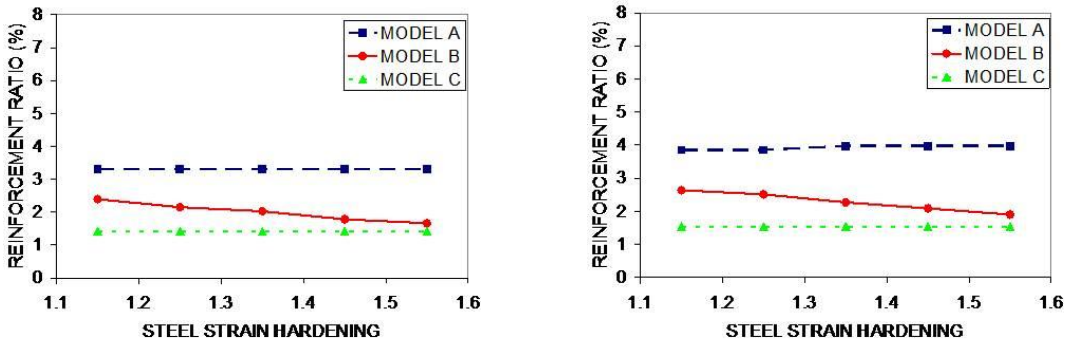

(a) (b)

Fig. 12 Variation of the longitudinal reinforcement demand with the reinforcing bar steel strain hardening f_{ul}/f_{yl} for the (a) circular and (b) square cross-section

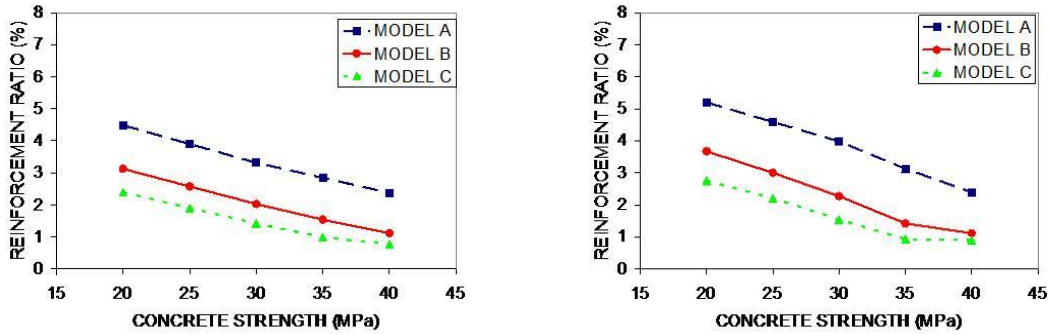

(a) (b)

Fig. 13 Variation of the longitudinal reinforcement demand with the concrete strength for the (a) circular and (b) square cross-section

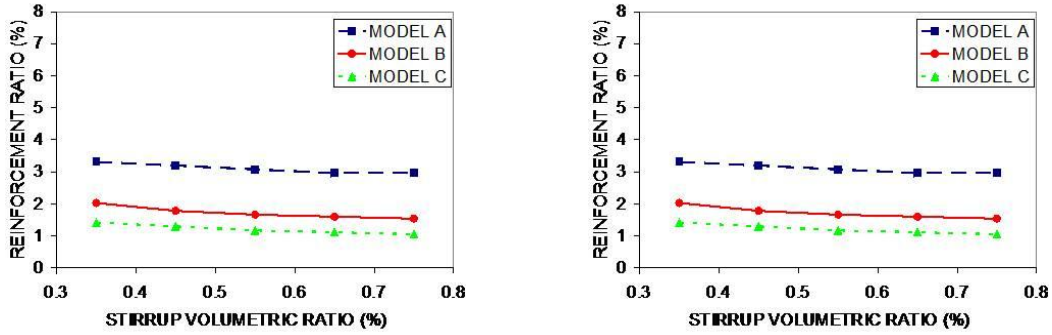

(a) (b)

Fig. 14 Variation of the longitudinal reinforcement demand with the transverse reinforcement volumetric ratio for the (a) circular and (b) square cross-section

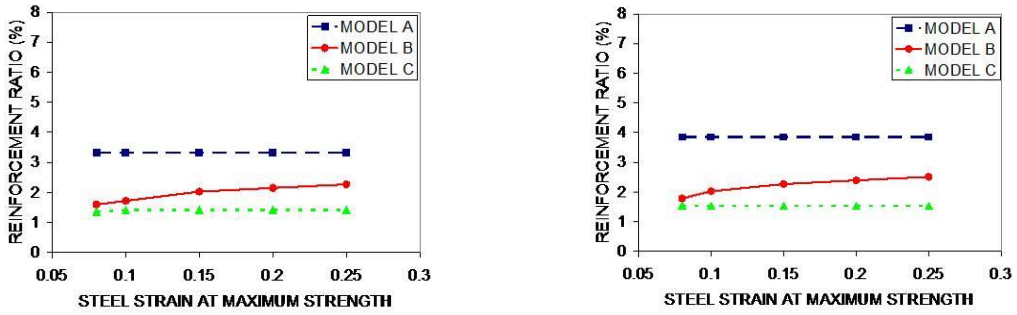

(a) (b)

Fig. 15 Variation of the longitudinal reinforcement demand with the longitudinal reinforcement strain at maximum strength ε_{su} for the (a) circular and (b) square cross-section

4.2.7 The concrete strength f_c

Herein, the influence of concrete strength f_c on ρ_l demand is investigated. For this cause, the basic design example is solved for five different concrete strengths f_c=20 MPa, 25 MPa, 30 MPa, 35 MPa and 40 MPa. Fig. 13 shows that all models predict significant decrease in ρ_l demand as f_c increases. This is explained by the fact that as f_c increases the curvature demand φ_d for the same limiting material strains increases since the neutral axis depth decreases. Hence, the displacement demand Δ_d increases and by Eq. 14 the design base shear V_B also decreases. In addition, moment capacity M_{cap} for the same ρ_l increases as f_c increases.

4.2.8 The transverse reinforcement volumetric ratio ρ_w

In traditional design of R/C members, there is no direct connection between ρ_l demand and the transverse reinforcement volumetric ratio ρ_w. To investigate this connection in DDBD for limiting material strains, the basic design example is solved for five different values of ρ_w=0.35%, 0.45%, 0.55%, 0.65% and 0.75%

It can be seen in Fig. 14 that, for all models, as ρ_w increases ρ_l demand decreases (in some cases up to 30%). This is due to the fact that the confining effect of the transverse reinforcement enhances the critical cross-section compression zone and the neutral axis depth becomes smaller for the same limiting strain. In this way, φ_d and subsequently Δ_d increase driving to smaller ρ_l demands.

4.2.9 The longitudinal reinforcement strain at maximum strength ε_{su}

Depending on the steel class, ε_{su} may range from 0.05 to 0.25. This parameter affects significantly the stress developed by the longitudinal reinforcement in the inelastic range. To examine the influence of ε_{su} on the ρ_l demand, the basic design example is solve for five different values of ε_{su}=0.08, 0.10, 0.15, 0.20 and 0.25. The reinforcement yield strength f_{yl} and strain hardening remain 500MPa and 1.35 respectively.

Fig. 14 shows that models A and C predict almost the same result for ρ_l for all different values of ε_{su}. However, model B predicts considerable increase of ρ_l as ε_{su} increases. This is because of the fact that as ε_{su} increases, for the same limiting material strains, the inelastic stress of the longitudinal reinforcement is reduced. Hence, the inelastic anchorage length L_{sh} decreases causing

significant decrease of the fixed end rotation generated by anchorage slip effect. Consequently, displacement demand Δ_d decreases and required longitudinal reinforcement increases. Again, this observation sets the need for modeling explicitly anchorage slip effect in DDBD for limiting material strains.

4.2.10 The bond strength

In the previous designs, the bond strength is taken by the Lehman and Moehle (1998) experimental observations for well confined R/C bridge columns. However, the bond strength may be different for various reasons like the confining reinforcement along the anchorage length, the quality of construction, the anchorage bar diameter and relative rib area the transverse pressure and others. To examine the sensitivity of ρ_l demand to the bond strength along the anchorage length, the bond strength of the basic design example is reduced by 10%, 20%, 30%, 40% and 50%.

Fig. 16 shows that while models A and B are independent of the assumed bond strength, the

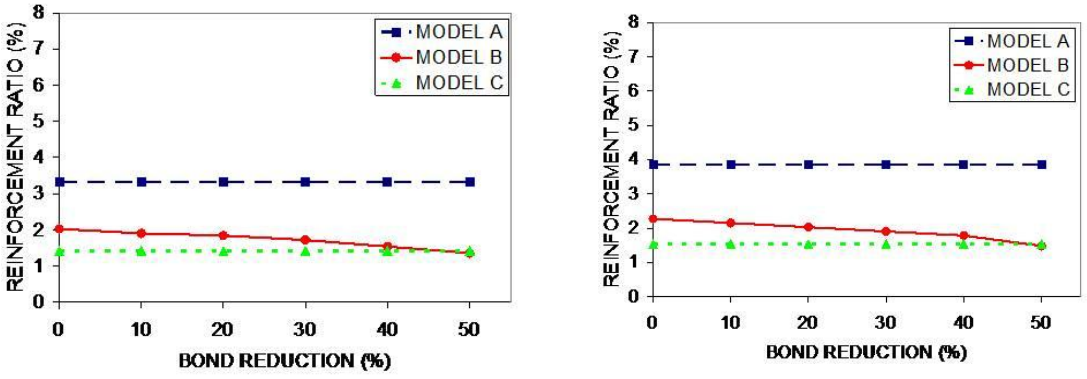

(a) (b)

Fig. 16 Variation of the longitudinal reinforcement demand with the bond strength reduction for the (a) circular and (b) square cross-section

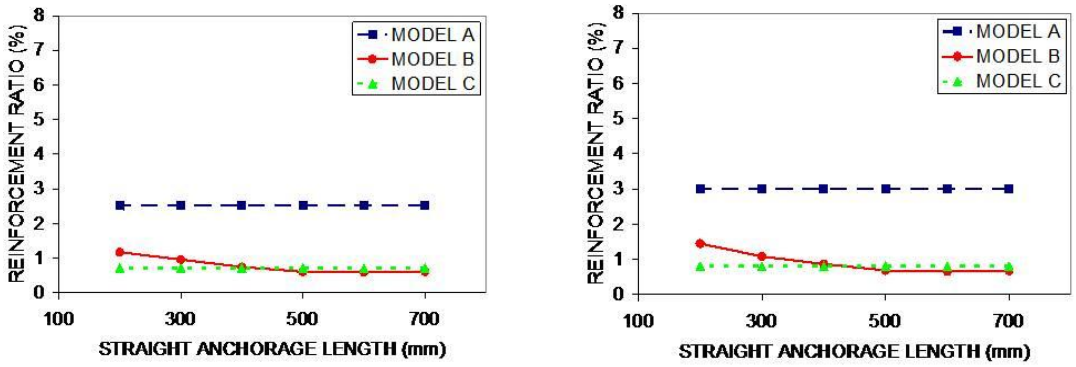

(a) (b)

Fig. 17 Variation of the longitudinal reinforcement demand with the straight anchorage length for hooked anchorages and the (a) circular and (b) square cross-section

predictions of model B are significantly influenced by this assumption. In particular, as bond strength decreases fixed end rotations caused by anchorage slip increase yielding higher values of Δ_d and consequently lesser ρ_l demands. This effect may be taken into account only by modeling explicitly anchorage slip phenomenon.

4.2.11 The straight anchorage length for hooked anchorages

In the previous, the anchorage is assumed straight and the anchorage length is considered as adequate to avoid brittle pullout failures. However, in many cases, the required straight anchorage length may not be applied (e.g. footings with small depths) and hooked anchorages are assigned.

In this case, the spread of bar deformations along the anchorage length is terminated at the location of the end-hook. Furthermore, the hook local slip is added to the total slip of the anchored bar (Alsiwat and Saatcioglu 1992).

To investigate the influence of the straight anchorage length $L_{straight}$ in the case of hooked anchorages, the basic design example is solved for six different values of $L_{straight}$=200 mm, 300 mm, 400 mm, 500 mm, 600 mm and 700 mm. Furthermore, to magnify anchorage slip effect the bar diameter and strain hardening are set equal to 25 mm and 1.55 respectively.

As illustrated in Fig. 17, the ρ_l demands predicted by the model B tend to increase for very small straight anchorage lengths. This is because the end-hook prevents anchored bars strains to expand. For straight anchorage lengths longer than $L_{straight}$=500 mm, ρ_l demand stabilizes. This means that the end-hook does not influence anchorage slip effect after this length.

5. Conclusions

Direct displacement-based design for limiting material strains represents an innovative design methodology, which connects directly the level of structural damage in the plastic hinge region to the design strength. This design approach requires an iterative analytical procedure, which may increase considerably the computational effort. For this reason, a new computer application is developed in this study, named RCCOLA-DBD, which automates calculation of longitudinal reinforcement demand for R/C cantilever members according to this design proposal.

In addition, the design strength, derived by DDBD methodology, is strongly affected by the displacement demand for the target material strains, which, in turn, may significantly be influenced by the fixed end rotation generated by anchorage slip at the cantilever base. To be consistent with this level of importance, it is proposed herein that anchorage slip effect is taken explicitly into account in the analytical design.

To achieve this goal, the Alsiwat and Saatcioglu (1992) analytical procedure is adopted in this study to evaluate the base moment vs. fixed end rotation envelope response. This methodology has been proven to provide adequate correlation with the experimental evidence, while it remains simple enough in order to be easily incorporated in seismic design of R/C members. The adopted analytical procedure is further improved herein in order to account for nonlinearity of the reinforcing steel strain-hardening response.

Next, by applying RCCOLA-DBD, numerous designs are conducted to study the influence of various parameters on DDBD for limiting material strains reinforcement demand ρ_l. It is shown that ρ_l demand sharply decreases as the limiting concrete ε_{cd} and steel ε_{sd} strains increase. Furthermore, for the same values of ε_{cd} and ε_{sd}, ρ_l demand rapidly decreases as the cantilever height, the longitudinal reinforcement yielding strength and the concrete strength increase. Finally,

ρ_l demand, again for the same limiting material strains, considerably decreases as the longitudinal reinforcing steel bar diameter and ratio of ultimate to yield strength increase, the transverse reinforcement volumetric ratio increases, the straight anchorage length for hooked anchorages increases, the longitudinal reinforcing steel strain at maximum strength decreases and the bond capacity along the anchorage length reduces.

In all these parametric designs, three different analytical models are examined. The first model ignores anchorage slip effect. The second model considers explicitly anchorage slip effect through the procedure proposed in this study. Lastly, the third model accounts indirectly for anchorage slip effect by the application of the equivalent plastic hinge length approach.

By comparing these three models, it is proven that anchorage slip influences strongly reinforcement demand and should definitely be included in the analytical procedure. Significant differences also arise when anchorage slip effect is included in the plastic hinge length and when it is determined explicitly by the suggested methodology. The latter approach advantages over the former because it can take into consideration additional design parameters like the reinforcing steel strain-hardening response, the concrete strength, the steel strain at maximum strength, the bond resistance along the anchorage length and the existence of end-hooks.

References

Alsiwat, J. and Saatcioglu, M. (1992), "Reinforcement anchorage slip under monotonic loading", *J. Struct. Eng*., **118**(9), 2421-2438.

Beyer, K., Dazio, A. and Priestley, M.J.N. (2011), "Shear deformations of slender R/C walls under seismic loading", *ACI Struct. J*., **108**(2), 167-177.

Calvi, G.M. and Sullivan, T.A. (2009), *Model code for the displacement based seismic design of structures*, IUSS Press, Pavia, Italy.

Dwairi, H.M., Kowalsky, M.J. and Nau, J.M. (2007), "Equivalent viscous damping in support of direct displacement-based design", *J. Earthq. Eng*., **11**(4), 512-530.

Fardis, M.N. (2009), *Seismic design, assessment and retrofitting of concrete buildings*, Springer.

fib Task Group 7.1 (2003), *Seismic assessment and retrofit of R/C buildings*, fib Bull. 24, Lausanne.

fib Task Group 7.2 (2003), *Displacement-based seismic design of reinforced concrete buildings*, fib Bull. 25, Lausanne.

Filippou, F. (1985), *A simple model for reinforcing bar anchorages under cyclic excitations*, Rep. EERC-85/05, Univ. of California, Berkeley.

Grant, D.N., Blandon, C.A. and Priestley, M.J.N. (2005), *Modeling inelastic response in direct displacement-based design*, Report 2005/03, IUSS Press, Pavia, Italy.

Kappos, A.J. (1991), "Analytical prediction of the collapse earthquake for R/C buildings: suggested methodology", *Earthq. Eng. Struct. D*., **20**(2), 167-176.

Kappos, A.J. (2002), *RCCOLA-90: Program for the inelastic analysis of R/C cross sections*, Imperial College, London.

Lehman, D. and Moehle, J.P. (1998), *Seismic performance of well confined concrete bridge columns*, PEER Report 1998/01, Univ. of California, Berkeley.

Lowes, L. and Altoontash, A. (2003), "Modeling reinforced concrete beam-column joints subjected to seismic loading", *J. Struct. Eng*., **129**(12), 1686-1697.

Ma, S.M., Bertero, V.V. and Popov, E.P. (1976), *Experimental and analytical studies on hysteretic behaviour of R/C rectangular and T-beam*, Report EERC 76-2, University of California, Berkeley.

Mahin, S.A. and Bertero, V.V. (1977), *RCCOLA: A computer program for reinforced concrete column analysis - user's manual and documentation*, Department of Civil Engineering, University of California, Berkeley.

Mander, J.B., Priestley M.J.N. and Park, R. (1986), "Theoretical stress- strain model for confined concrete", *J. Struct. Eng*., **114**(8), 1804-1825.
Mergos, P.E. and Kappos, A.J. (2008), "A distributed shear and flexural flexibility model with shear-flexure interaction for R/C members subjected to seismic loading", *Earthq. Eng. Struct. D.*, **37**(12), 1349-1370.
Mergos, P.E. and Kappos, A.J. (2010), "Seismic damage analysis including inelastic shear-flexure interaction", *B. Earthq. Eng*., **8**(1), 27-46.
Mergos, P.E. (2011), *Assessment of seismic behaviour of existing R/C structures*, PhD Thesis, Aristotle University of Thessaloniki, Greece.
Mergos, P.E. and Kappos, A.J. (2012), "A gradual spread inelasticity model for R/C beam-columns, accounting for flexure, shear and anchorage slip", *Eng. Struct*., **44**, 94-106.
Otani, S. and Sozen, M. (1972), *Behavior of multistory R/C frames during earthquakes*, Struct. Res. Series 392, University of Illinois, Urbana.
Park, R. and Sampson, R.A. (1972), "Ductility of reinforced concrete column sections in seismic design", *ACI Struct. J*., **69**(9), 543-551.
Paulay, T. and Priestley, M.J.N. (1992), *Seismic design of reinforced concrete and masonry buildings*, John Wiley & Sons, New York.
Priestley, M.J.N. (1993), "Myths and fallacies in earthquake engineering – conflicts between design and reality", *B. NZSEE*, **26**(3), 329-341.
Priestley, M.J.N. and Kowalsky, M.J. (2000), "Direct-displacement based seismic design of concrete buildings", *B. NZSEE*, **33**(4), 421-444.
Priestley, M.J.N., Calvi, G.M. and Kowalsky, M.J. (2007), *Displacement-based seismic design of structures*, IUSS Press, Pavia, Italy.
Saatcioglu, M. and Ozcebe, G. (1989), "Response of reinforced concrete columns to simulated seismic loading", *ACI Struct. J*., **86**(1), 3-12.
Sezen, H. and Setzler, E.J. (2008), "Reinforcement anchorage slip under monotonic loading", *ACI Struct. J*., **105**(3), 280-289.
Shibata, A. and Sozen, M. (1976), "Substitute structure method for seismic design in reinforced concrete", *ASCE J. Struct. Eng*., **102**(1), 1-18.
Soroushian, P., Kienuwa, O., Nagi, M. and Rojas, M. (1988), "Pullout behaviour of hooked bars in exterior beam-column connections", *ACI Struct. J*., **85**(3), 269-276.

CC